Journal of Magnetic Resonance **143,** 208–212 (2000)
doi:10.1006/jmre.1999.1982, available online at http://www.idealibrary.com on IDEAL®

COMMUNICATIONS

Volume Selective Detection by Weighted Averaging of Constant Tip Angle Scans

Igor Serša[1] and Slobodan Macura[2]

Department of Biochemistry and Molecular Biology, Mayo Graduate School, Mayo Clinic and Mayo Foundation, Rochester, Minnesota 55905

Received June 28, 1999; revised November 10, 1999

We propose a method to improve the sensitivity in volume selective detection based on the CARVE excitation sequence (I. Serša and S. Macura, *J. Magn. Reson.* 135, 466–477 (1998)) which consists of signal acquisition with constant tip angle excitation and a short phase-encoding gradient pulse. Volume selectivity is achieved using the weighted average of a number of scans whose weights and gradient steps are determined by the shape of the excitation profile. The method is particularly useful for broadband volume selective detection of insensitive spins where the volume selection can be merged with the standard signal averaging process, without compromising the excitation bandwidth or sensitivity. © 2000 Academic Press

Key Words: **spectroscopic imaging; volume selective excitation; volume selective detection.**

Volume selective excitation (VSE) provides the signal from the region of interest much faster than the uniform excitation and imaging of the whole sample (*1–4*). This stems from a reduction in the dimensionality and subsequent decrease in the total experiment time and data size. Whereas simple shapes (cubes or spheres) can be excited in a straightforward manner, complex shapes require sophisticated pulse sequences and data reduction techniques. For example, complex shapes can be excited by spectral–spatial selective pulses which are based on the simultaneous application of shaped radiofrequency (RF) and gradient waveforms (*5–7*). The basic disadvantage of spectral–spatial selective pulses is that additional data processing (regriding) is necessary prior to standard Fourier transformation. This arises because of the inherent limitations in the gradient hardware. Additionally, because of long excitation time the spectral–spatial selective pulses are sensitive to off-resonance effects, and the desired excitation profile can be obtained for on-resonance spins only.

Volume selective detection (VSD) methods also enable signal localization to objects with complex shapes. VSD methods are derived from spectroscopic imaging techniques (*8, 9*) utilizing *k*-space signal weighting. Signals at different steps of the phase-encoding gradient are summed with different weights, and this restricts the signal to the desired region. Signal weighting can be done online during acquisition by varying the tip angle of the excitation pulse (*10, 11*), by varying the number of signal averages at each step of phase-encoding gradient (*12*), or in postprocessing, by numerical signal weighing (*13, 14*). Because VSD methods use broadband signal excitation, they are also insensitive to off-resonant spins. The *k*-space signal weighting is also used in imaging for reduction of the Gibbs artifact (*15–17*).

We have proposed a similar technique for volume selective excitation, CARVE (*18, 19*), which uses discrete RF pulses (generalized DANTE sequence (*20*)) in combination with discrete gradient steps. The basic advantage of CARVE is that it is linear and consequently the results of several experiments can be summed to generate an excitation profile of the desired (arbitrary) shape and spatial and spectral resolution (*21*). In this Communication we describe a method that achieves considerable improvement in the sensitivity of CARVE-based VSD by utilizing a weighted average of the signals acquired with constant tip angle (CTA) excitation.

The theoretical background of the CARVE method is described in detail elsewhere (*22*). Here we outline the elements relevant for VSD. CARVE is based on the Fourier transform relationship between the excitation profile $P_N(\mathbf{r}_n)$ defined in a D-dimensional cube (with sides L by a matrix of $N = M^D$ equidistant points $\mathbf{r}_n$ that span a rectangular grid) and the complex RF pulses $\Theta_N(\mathbf{k}_l)$ (*5, 23, 24*),

$$\Theta_N(\mathbf{k}_l) = \frac{1}{N}\sum_{n=0}^{N-1} P_N(\mathbf{r}_n)\exp(-i\mathbf{r}_n\mathbf{k}_l). \qquad [1]$$

The complex RF pulses $\Theta_N(\mathbf{k}_l)$ which depend on the *k*-space vectors, $\mathbf{k}_l$, are defined by the tip angle θ_l and phase φ_l:

[1] On leave from the Department of Solid State Physics, Josef Stefan Institute, 1000 Ljubljana, Slovenia.

[2] To whom correspondence should be addressed. Fax: (507) 284-8433. E-mail: macura@mayo.edu.

1090-7807/00 $35.00

$\Theta_N(\mathbf{k}_l) = \theta_l \exp(i\varphi_l)$. Similarly, an ideal profile $P_N(\mathbf{r}_n)$ is the Fourier transform of the complex RF pulses $\Theta_N(\mathbf{k}_l)$. This can be also interpreted as a projection of the profile onto N basis functions (harmonics) $\exp(i\,\mathbf{r}_n\mathbf{k}_l)$ with weights $\Theta_N(\mathbf{k}_l)$ (*21*). In CARVE each event consisting of a short RF pulse followed by a gradient pulse generates one basis function. Thus, to excite the profile $P_N(\mathbf{r}_n)$, defined with N basis functions, one needs N RF pulses and N gradient steps (k-space coordinates). Because N may be prohibitively large for practical pulse sequence design, it is necessary to reduce the number of RF pulses to a reasonable size N', which yields a good approximation of the ideal profile:

$$P_{N'}(\mathbf{r}_n) = \sum_{l=0}^{N'-1} \Theta_N(\mathbf{k}_l) \exp(+i\mathbf{r}_n\mathbf{k}_l). \qquad [2]$$

The summation in Eq. [2] is over the N' selected coefficients $\Theta_N(\mathbf{k}_l)$ and may provide significant savings in CARVE experiment time.

Equation [2] does not specify the order in which the summation is performed. Neglecting relaxation during the sequence and the size of the excitation bandwidth, for on-resonance magnetization the same result would be obtained if the whole N'-pulse sequence is executed in a single experiment (VSE) or in a series of N' one-pulse scans (VSD). Equation [2] only stipulates that the desired excitation profile be obtained by coaddition of signals excited by RF pulses $\Theta_N(\mathbf{k}_l)$ applied at the respective k-space points, $\mathbf{k}_l$. However, the excitation spectral bandwidth depends on the pulse train duration and for broadband excitation a series of N' one-pulse scans is required. Thus, broadband VSD consists of coaddition of signals from N' scans, each consisting of one RF pulse and one gradient step (*21*).

One way to reduce the number of coefficients from N to N' is to select N' Θ-coefficients with the largest tip angles θ. If the number of scans necessary to achieve the desired signal-to-noise ratio (SNR) is larger than N', then the implementation of VSD may be invisible because each scan can be acquired as one summation term from Eq. [2]. With more scans a larger number of coefficients N' can be used with an improvement of the SNR and spatial resolution. However, because of the decrease in the average tilt angle with an increasing number of coefficients, such a simple picture is not quite true and a more detailed analysis of SNR is warranted.

The small tip angle excitation theory (*23*) here expressed by Eqs. [1,2] implies that the total tip angle, θ_{total}, within the profile is small ($\leq 5°$). Therefore, in our analysis we assume that the CARVE tip angles, θ_l, are sufficiently small so that θ_{total} satisfies the small tip angle condition. We also assume that the noise is independent of the receiver gain and that the latter is set to appropriately fill the analog to digital converter. If the signal from a unit volume inside the excitation profile, in a single scan experiment with N' coefficients, is S_0 and corresponding noise σ_0, then with N' scans the SNR is $(S_0/\sigma_0)\sqrt{N'}$. In the experiment with N' one-pulse scans, with the tip angles θ_l from the same set, and the same receiver gain, the SNR $= (S_0/\sigma_0)/\sqrt{N'}$. The SNR in repeated scans decreases because the total magnetization is summed to the same value as that in a single N'-pulse scan, and in repeated scans more noise is added. Since in a one-pulse scan the magnetization is tipped for an individual tip angle θ_l (in contrast to a N'-pulses scan where the total tip angle in each scan is θ_{total}), the receiver gain could be increased to accommodate a signal from the scan with a maximal tip angle $\theta_{\max}$. Then the SNR of the experiment with N' one-pulse scans with variable tip angle (VTA) improves to

$$\text{SNR}_{\text{VTA}} = \frac{\theta_{\text{total}}}{\theta_{\max}\sqrt{N'}}\frac{S_0}{\sigma_0}. \qquad [3]$$

Because the average tip angle $\langle\theta\rangle$ ($\langle\theta\rangle = \sum_{l=0}^{N'-1}\theta_l/N'$) is less than or equal to $\theta_{\max}$, the experiment with N' one-pulse scans always has a lower SNR than N' repeated experiments of N'-pulse scans.

The SNR can be maximized if the N' one-pulse scans are repeated with a CTA excitation pulse θ_c (then $\theta_c = \theta_{\max}$) and constant phase φ_0, but with variable gradients as required by Eq. [2], and if the receiver gain is optimized for a given pulse angle. In such an experiment with maximized SNR all information about the geometry of the excitation profile is lost, because all of the Θ-coefficients are rendered equal. However, the original coefficients can be restored after data acquisition by the weighted averaging of individual scans. The weights in the averaging are complex numbers with magnitudes proportional to the tilt angles θ and phases equal to the RF phase φ. The weighting scales both the signal and the noise, preserving their ratio in the individual scans. The weighted averaging scales the total signal to the level of the signal in an N'

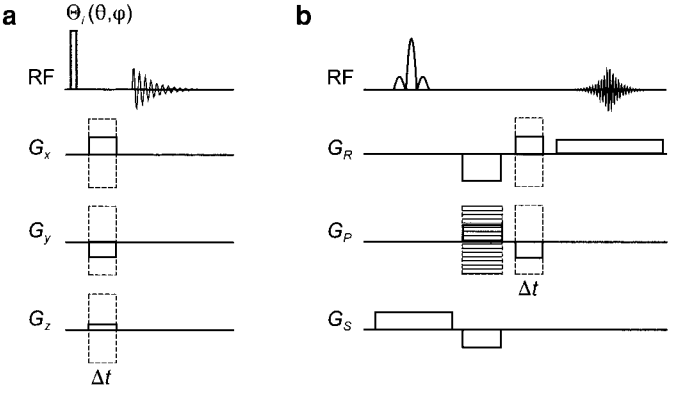

FIG. 1. Pulse sequences for broadband volume selective excitation: (a) actual sequence; (b) the gradient-echo implementation for visual inspection of experimental excitation profiles.

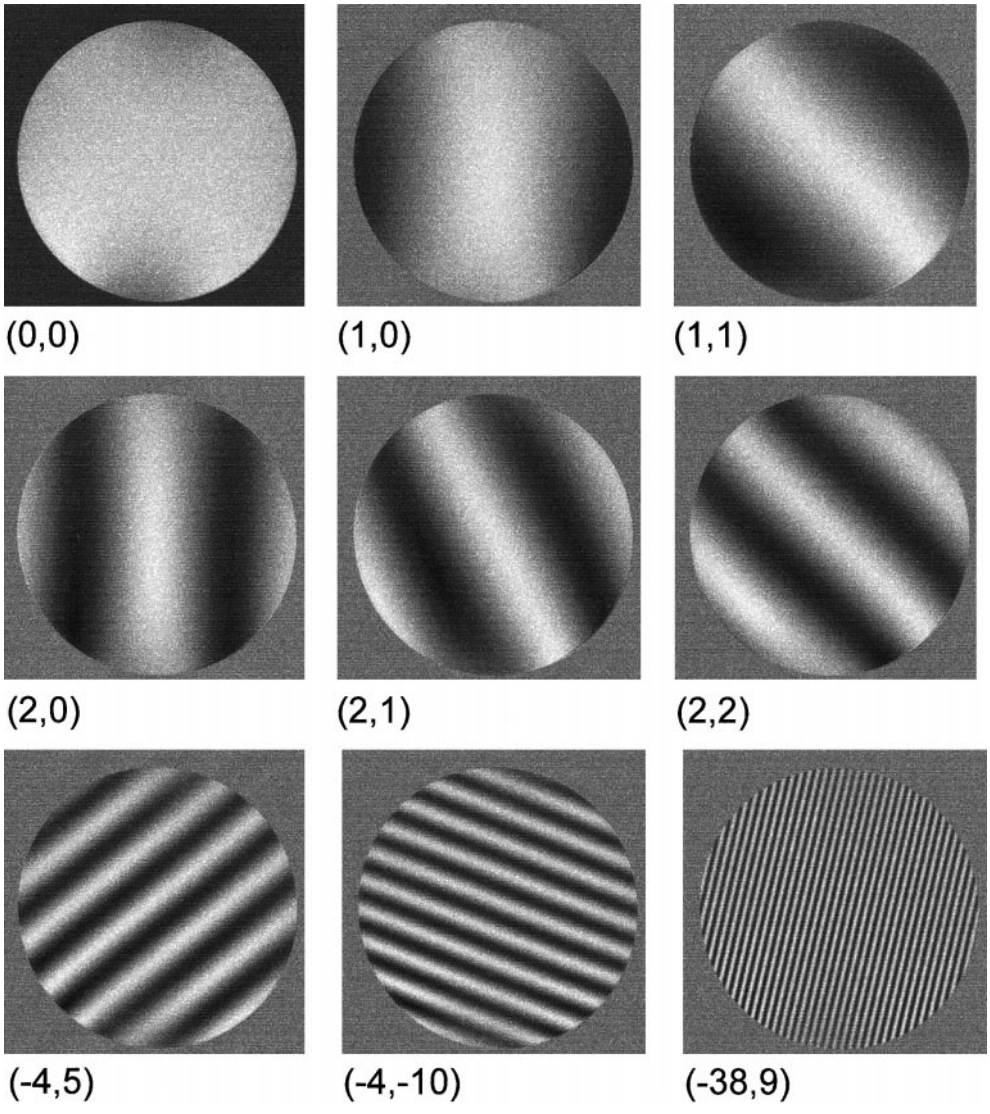

FIG. 2. Phase encoding in the constant tip angle experiment. A 10-mm NMR tube is imaged with a constant tip angle pulse and different phase-encoding gradients. Each gradient step corresponds to one k-space point (k_x, k_y). Only the real part of the image is shown, thus the phases are the same for centrosymmetric points. The images also represent the basis functions whose weighted sum, Eq. [2], gives the desired profile. For real profiles the weighting coefficients of each centrosymmetric k-space points are complex conjugates of each other.

one-pulse experiment with variable tip angle, $S_0\ \theta_{\text{total}}/\theta_{\text{max}}$ and the noise to $\sigma_0\ (\sqrt{\sum_{l=0}^{N'-1}\theta_l^2})/\theta_{\text{max}}$ which yields

$$\text{SNR}_{\text{CTA}} = \frac{\theta_{\text{total}}}{\sqrt{\sum_{l=0}^{N'-1}\theta_l^2}}\frac{S_0}{\sigma_0}. \qquad [4]$$

In comparison to the SNR of the variable tip angle experiment, the total improvement is

$$f = \frac{\text{SNR}_{\text{CTA}}}{\text{SNR}_{\text{VTA}}} = \frac{\theta_{\text{max}}}{\sqrt{\sum_{l=0}^{N'-1}\theta_l^2/N'}} = \frac{\theta_{\text{max}}}{\sqrt{\langle\theta^2\rangle}}. \qquad [5]$$

The improvement factor, f, depends on the shape of the actual excitation profile. It is always greater than 1 and can be as high as 100 for high-definition (large N'), delocalized ($\theta_{\text{max}} \gg \langle\theta\rangle$) profiles. Thus, data acquisition with constant tip angle and subsequent weighted summation of the recorded signals produces broadband VSD with an improved SNR.

The pulse sequence for broadband VSD consists of a single event from the CARVE sequence (a small tip angle pulse followed by the gradient step) and data acquisition, as depicted in Fig. 1a. In a standard experiment the receiver gain is optimized using the scan with maximal tip angle and in subsequent scans the gradient magnitude, the RF tip angle, and phase are read from a list generated individually for each

profile shape. These scans are coadded. In the CTA experiments the RF tip angle is kept constant and the receiver gain is optimized accordingly. Then, the gradient and RF phase values are changed in subsequent scans as in CARVE and scans are added with the weights proportional to their original tip angles.

To demonstrate the different properties of broadband VSD, we have incorporated the sequence into a standard gradient-echo imaging routine, as shown in Fig. 1b. For simplicity, we have performed experiments in two dimensions only. For constant gradient times Δt, the transverse magnetization created by the RF pulse is modulated by the applied gradients only. This modulation is depicted in Fig. 2 where a series of phase-sensitive images (cross-sections of a water-filled 10-mm NMR tube) are shown representing different combinations of x and y gradients. Each image represents the signal modulation at the indicated k-space point (since each gradient combination represents a distinct k-space point). All images were acquired with the same θ_0 RF pulse and thus represent a subset of basis functions over which the actual excitation profile is described (see Eq. [2]). In contrast to spectroscopic imaging where all the basis functions are used, CARVE uses a subset of the basis functions with the largest Θ-coefficients. Functions, having their Θ-coefficients below a selected threshold, have their magnitude set to zero. This provides enormous savings in data size and acquisition time since the subset is often orders of magnitude smaller than the original basis set. In return such a truncated set generates an approximate profile.

Since the CARVE profile approximation is based on simple elimination of the smallest Fourier coefficients (Eq. [2]), the generated approximate profile suffers from truncation errors (Gibbs phenomenon). However, these errors can be minimized by smoothing of the ideal profile using a low-pass filter. More complex methods can be used to select N' basis functions and to calculate their corresponding coefficients to generate less distorted approximations. While such methods are more computationally intensive, their output is better optimized. Then either a better approximation of the ideal profile may be obtained with the same number of basis functions or the similar approximation can be obtained with fewer basis functions.

The extent of the SNR improvement in the CTA experiment can be deduced from Fig. 3 which shows experimental images of the phantom obtained by the two methods. Figure 3a shows the original 256×256 pixel^2 phantom and Fig. 3b the image after smoothing (to avoid Gibbs phenomenon). Figures 3c and 3d show the experimental profiles obtained in the same experimental time with variable and constant tip angle, respectively. The experimental SNR enhancement factor in the CTA experiment of 11.5 is in good agreement with the theoretically predicted value of 11.9.

The basic disadvantage of the CTA experiment is that current commercial spectrometer software does not allow the rescaling of individual FIDs before coaddition. In our experiments we have collected the FIDs separately in a 2D manner and have coadded them with appropriate weights during signal processing. However, the weighted signal averaging could be easily implemented with minor software modifications.

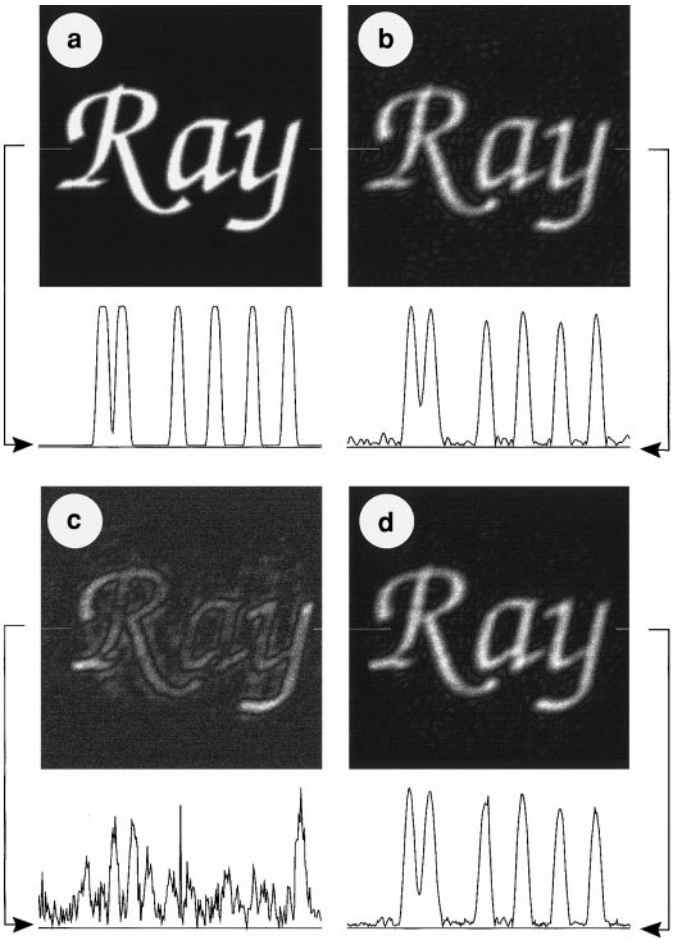

FIG. 3. Experimental demonstration of the SNR improvement in the constant tip angle (CTA) experiment: (a) 8-bit 256×256 ideal excitation profile; (b) the profile approximation with 1000 coefficients, Eq. [2]; (c) experimental profile with the variable tip angle (VTA) 1000 one-pulse scans; (d) experimental profile reconstructed by the weighted averaging of the 1000 one-pulse scans with CTA. Cross-sections shown below the respective images are taken from the same position within the images as indicated by the arrows.

With the widespread use of three-axis gradient probes, it is conceivable that weighted signal averaging can be beneficially used in any experiment where signal averaging is performed due to inherently poor SNR. For example, in the detection (direct or indirect) of insensitive nuclei using natural abundance, the weighted averaging scheme can be invisibly implemented to localize the signal to the region of interest. The proposed method is closely related to the partial Fourier imaging method (*12, 13*) in which weighting is achieved by varying the number of scans. For $N' = N$ the method is the same as the VSD method in which the spectroscopic imaging data set is multiplied by a filter function.

The experiments were performed on a Bruker Avance 300 wide-bore high-resolution spectrometer equipped with micro-imaging accessories on a 10-mm tube filled with water. To

eliminate the effects of finite gradient slew rates the time duration of each gradient step, Δt, was set at 1 ms. This also kept the gradient load within 18% of the maximal gradient, 90 mT/m vs 500 mT/m. The profiles in Fig. 2 were obtained by the gradient-echo imaging sequence with a field of view 10 mm, repetition rate 100 ms, imaging matrix size 256 $\times$ 256, and imaging time 25.6 s. The total experiment time to visualize the profile (Figs. 3c and 3d) was 1000 $\times$ 25.6 s, which is approximately 7 h. However, volume selective detection of a spectrum from a selected region at these parameters would take only 1000 $\times$ 100 ms = 100 s.

ACKNOWLEDGMENTS

We thank Drs. Elizabeth Kurian and Martin Moncrieffe for critical reading of the manuscript. We are also grateful to the reviewers for useful comments and suggestions.

REFERENCES

1. S. Mueller, W. P. Aue, and J. Seelig, Practical aspects of volume-selective excitation (vse) compensation sequences, *J. Magn. Reson.* **65,** 332–338 (1985).
2. W. P. Aue, S. Muller, T. Cross, and J. Seelig, Volume-selective excitation. A novel approach to topical NMR, *J. Magn. Reson.* **56,** 350–354 (1984).
3. D. Doddrell, J. Bulsing, G. Galloway, W. Brooks, J. Field, M. Irving, and H. Baddeley, Discrete isolation from gradient-governed elimination of resonances. DIGGER, a new technique for *in vivo* volume-selected NMR spectroscopy, *J. Magn. Reson.* **70,** 319–326 (1986).
4. D. M. Doddrell, W. M. Brooks, J. M. Bulsing, J. Field, M. G. Irving, and H. Baddeley, Spatial and chemical-shift-encoded excitation. SPACE, a new technique for volume-selected NMR spectroscopy, *J. Magn. Reson.* **68,** 367–372 (1986).
5. C. H. Meyer, J. M. Pauly, A. Macovski, and D. G. Nishimura, Simultaneous spatial and spectral selective excitation, *Magn. Reson. Med.* **15,** 287–304 (1990).
6. G. Morrell and A. Macovski, Three-dimensional spectral–spatial excitation, *Magn. Reson. Med.* **37,** 378–386 (1997).
7. D. Spielman, J. Pauly, A. Macovski, and D. Enzmann, Spectroscopic imaging with multi-dimensional pulses for excitation: SIMPLE, *Magn. Reson. Med.* **19,** 67–84 (1991).
8. A. A. Maudsley, S. K. Hilal, W. H. Perman, and H. E. Simon, Spatially resolved high resolution spectroscopy by "four-dimensional" NMR, *J. Magn. Reson.* **51,** 147–152 (1983).
9. T. R. Brown, B. M. Kincaid, and K. Ugurbil, NMR chemical shift imaging in three dimensions, *Proc. Natl. Acad. Sci. USA* **79,** 3523–3526 (1982).
10. G. A. Webb, R. W. Briggs, and T. H. Mareci, Volume-localized spectroscopy using selective Fourier transform by variable-tip-angle excitation, *J. Magn. Reson.* **94,** 174–179 (1991).
11. A. G. Webb, T. H. Mareci, and R. W. Briggs, Relative efficiencies of weighting methods for phase-encoded localized NMR, *J. Magn. Reson. B* **103,** 274–277 (1994).
12. T. H. Mareci and H. R. Brooker, High-resolution magnetic resonance spectra from a sensitive region defined with pulsed field gradients, *J. Magn. Reson.* **57,** 157–163 (1984).
13. H. R. Brooker, T. H. Mareci, and J. Mao, Selective Fourier transform localization, *Magn. Reson. Med.* **5,** 417–433 (1987).
14. T. H. Mareci and H. R. Brooker, Essential considerations for spectral localization using indirect gradient encoding of spatial information, *J. Magn. Reson.* **92,** 229 (1991).
15. J. H. den Boef, C. M. van Uijen, and C. D. Holzscherer, Multiple-slice NMR imaging by three-dimensional Fourier zeumatography, *Phys. Med. Biol.* **29,** 857–867 (1984).
16. D. L. Parker, G. T. Gullberg, and P. R. Frederick, Gibbs artifact removal in magnetic resonance imaging, *Med. Phys.* **14,** 640–645 (1987).
17. A. G. Webb and R. B. Clarkson, Sensitivity enhancement and reduction of Gibbs artifact in T_2-weighted imaging using variable tip angle excitation, *Magn. Reson. Med.* **21,** 308–312 (1991).
18. I. Sersa and S. Macura, Excitation of arbitrary shapes in nuclear magnetic resonance by a random walk in discrete *k*-space, *J. Magn. Reson. B* **111,** 186–188 (1996).
19. I. Sersa and S. Macura, Excitation of arbitrary shapes by gradient optimized random walk in discrete *k*-space, *Magn. Reson. Med.* **37,** 920–931 (1997).
20. G. A. Morris and R. Freeman, Selective excitation in Fourier transform nuclear magnetic resonance, *J. Magn. Reson.* **29,** 433–462 (1978).
21. I. Sersa and S. Macura, Excitation of complicated shapes in three dimensions, *J. Magn. Reson.* **135,** 466–477 (1998).
22. I. Sersa and S. Macura, Excitation of complex profiles by CARVE sequence: Accounting for spectral dispersion and relaxation, *J. Imag. Sci. Technol.* **10,** 225–241 (1999).
23. J. Pauly, D. Nishimura, and A. Macovski, A k-space analysis of small-tip-angle excitation, *J. Magn. Reson.* **81,** 43–56 (1989).
24. J. Pauly, D. Nishimura, and A. Macovski, A linear class of large-tip-angle selective excitation pulses, *J. Magn. Reson.* **82,** 571–587 (1989).